Density Field Dynamics Resolves the Penrose Superposition Paradox

Gary Alcock
Independent Researcher, Los Angeles, CA, USA
(Dated: September 19, 2025)

Penrose has argued that a quantum superposition of mass distributions leads to a structural inconsistency: in general relativity, each branch would source a distinct spacetime geometry, whereas quantum mechanics allows only a single state until collapse. We show that Density Field Dynamics (DFD), a scalar-field completion of Einstein's 1911–12 variable-c program, avoids this paradox entirely. In DFD there is no manifold branching: superposed mass distributions source a single classical (c-number) refractive field ψ, which governs both light ($n = e^{\psi}$) and matter ($\boldsymbol{a} = \frac{c^2}{2}\nabla\psi$). In the weak-field linear regime ($\mu \to 1$), ψ is the convex sum of the branch fields; in the full quasilinear regime, monotonicity of the crossover function μ ensures existence and uniqueness of a single solution. Thus DFD is structurally compatible with quantum superposition, unlike GR, and the decisive discriminator remains laboratory testability: the co-located cavity–atom redshift comparison at two altitudes, where GR predicts zero slope and DFD predicts a geometry-locked slope of $\mathcal{O}(\Delta\Phi/c^2) \sim 10^{-14}$ per 100 m.

I. INTRODUCTION

Penrose has long emphasized a tension between general relativity (GR) and quantum mechanics (QM) [1, 2]. If a macroscopic object is placed in spatial superposition, GR demands that each branch source its own spacetime curvature, while QM maintains only a single quantum state until measurement. This "two spacetimes vs. one Hilbert space" contradiction underpins Penrose's proposal that gravity induces wavefunction collapse.

Density Field Dynamics (DFD) [13–15] replaces curved spacetime with a single classical (c-number) scalar refractive field $\psi(\boldsymbol{x})$. Photons propagate with index $n = e^{\psi}$, matter accelerates as $\boldsymbol{a} = \frac{c^2}{2}\nabla\psi$, and ψ obeys the quasilinear elliptic equation

$$\nabla\cdot\left[\mu\left(\frac{|\nabla\psi|}{a_\star}\right)\nabla\psi\right] = -\frac{8\pi G}{c^2}\left(\rho - \bar{\rho}\right), \tag{1}$$

with $\mu \to 1$ in the weak-field regime (and $a_\star$ the characteristic deep-field acceleration scale). Normalization reproduces GR's weak-field optical tests [3], while the μ-family enforces scale symmetry, ellipticity, and convex energy density [9].

II. SUPERPOSITION SOURCES IN DFD

Let the quantum state of a mass distribution be $|\Psi\rangle$, with density operator $\hat{\rho}(\boldsymbol{x})$. The effective source entering (1) is the expectation value

$$\rho_{\text{eff}}(\boldsymbol{x}) = \langle\Psi|\hat{\rho}(\boldsymbol{x})|\Psi\rangle. \tag{2}$$

For a superposition of two localized packets $|L\rangle, |R\rangle$ with $|\Psi\rangle = a|L\rangle + b|R\rangle$,

$$\rho_{\text{eff}} \simeq |a|^2\rho_L + |b|^2\rho_R + 2\,\mathrm{Re}(a^* b\,\rho_{LR})\,, \tag{3}$$

where the interference term ρ_{LR} is exponentially suppressed for well-separated packets. In the linear (Poisson) regime ($\mu \to 1$), the field solution is

$$\psi \simeq |a|^2\psi_L + |b|^2\psi_R, \tag{4}$$

a convex sum of branch fields. In the full nonlinear regime, monotone μ ensures uniform ellipticity; existence and uniqueness follow by variational methods (Sec. VII). Thus there is always a single ψ field—a weighted combination of branch contributions—ensuring no manifold branching.

A. Semiclassical sourcing (but not semiclassical GR)

DFD sources a *classical* scalar field ψ by $\rho_{\text{eff}} = \langle\hat{\rho}\rangle$, yet the geometry is never promoted to an operator; there is no $\hat{g}$. This is not the semiclassical Einstein equation $G_{\mu\nu} = 8\pi G\langle\hat{T}_{\mu\nu}\rangle$. Instead, the optical metric for light is $n = e^{\psi}$

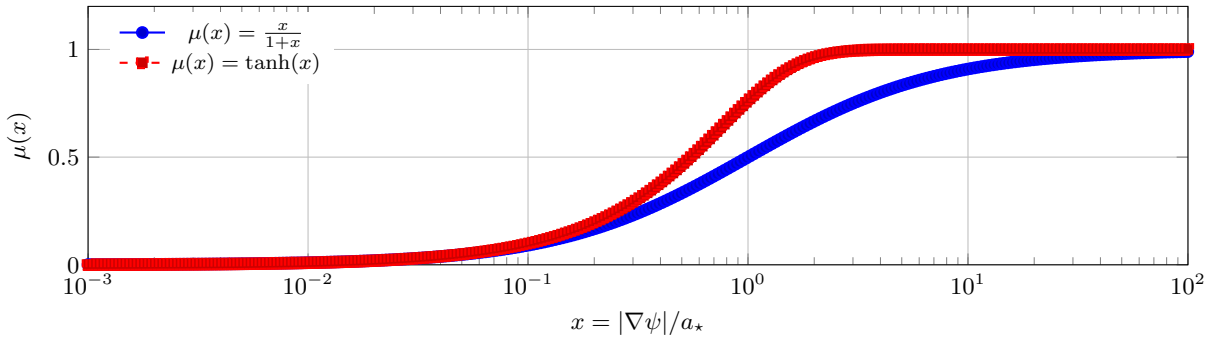

FIG. 1. Representative crossovers: linear for $x \gg 1$, scaling $\mu \sim x$ for $x \ll 1$. Both preserve a unique classical ψ.

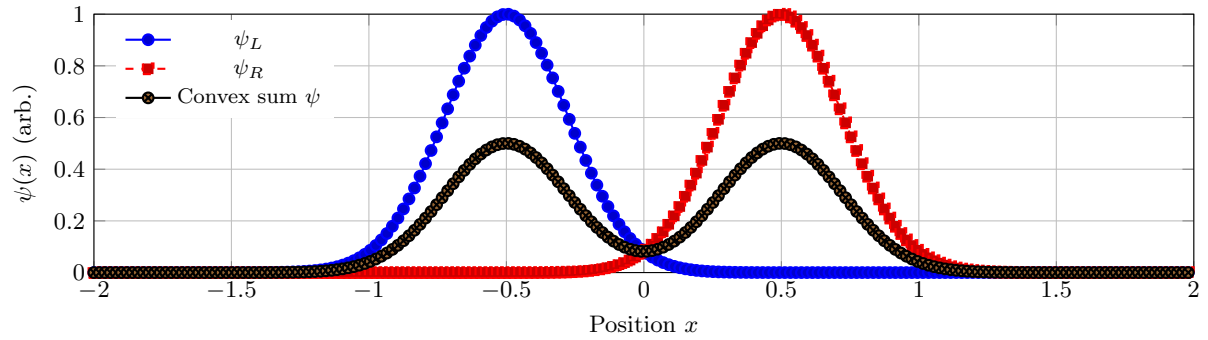

FIG. 2. Illustrative ψ-profiles for two separated packets in 1D. Only the convex-sum field exists in DFD.

(Euclidean background with refractive structure), and matter follows $\boldsymbol{a} = \frac{c^2}{2}\nabla\psi$. Hence no operator-valued geometry arises, and Penrose's paradox does not materialize.

B. Linear vs. Nonlinear Regimes

DFD's $\mu(x)$ crossover unifies two limits with a single PDE and a single ψ: (i) the high-gradient (solar-system) regime $\mu \to 1$, where the equation reduces to a linear Poisson problem; and (ii) the deep-field (galactic) regime $\mu(x) \sim x$, which yields scale-free behavior $|\nabla\psi| \propto 1/r$ and flat rotation curves. In both regimes ψ is a classical field determined by ρ_{eff}; no operator-valued geometry arises.

C. Worked example: superposed grain of sand

Consider $m \sim 10^{-7}\,\text{kg}$ in a spatial superposition with branch centers separated by $d \sim 1\,\mu\text{m}$. In GR, two geometries are implicated. In DFD, $\rho_{\text{eff}} \approx \frac{1}{2}(\rho_L + \rho_R)$ and the weak-field solution is $\psi = \frac{1}{2}(\psi_L + \psi_R)$ by (4). The acceleration field $\boldsymbol{a} = (c^2/2)\nabla\psi$ and optical index $n = e^{\psi}$ are single-valued; no paradox arises.

III. QUANTUM EVOLUTION AND CONTINUITY

Matter wavefunctions evolve with

$$i\hbar\partial_t\Psi = -\frac{\hbar^2}{2m}\,\nabla\cdot\big(e^{-\psi}\nabla\Psi\big) + m\Phi\,\Psi, \qquad \Phi = -\tfrac{c^2}{2}\psi. \tag{5}$$

Define the current

$$\boldsymbol{J} = \frac{\hbar}{2mi}\,e^{-\psi}\big(\Psi^*\nabla\Psi - \Psi\nabla\Psi^*\big). \tag{6}$$

TABLE I. Illustrative error budget for $\Delta R/R$ at the 10^{-14} per 100 m level.

Systematic	Target (frac.)	Control handle
Cavity dispersion (dual-λ)	$\lesssim 3\times10^{-15}$	Dual-wavelength bound
Cavity elastic sag / flips	$\lesssim 3\times10^{-15}$	180° orientation flips + model
Atom transition sensitivity	$\lesssim 3\times10^{-15}$	Co-trapped species calibration
Comb transfer noise	$\lesssim 1\times10^{-16}$	Stabilized links + counters
Thermal gradients / birefringence	$\lesssim 3\times10^{-15}$	Active stabilization; polarization checks

Multiplying (5) by Ψ^* and subtracting the conjugate equation yields

$$\partial_t|\Psi|^2 + \nabla\cdot\boldsymbol{J} = 0, \tag{7}$$

so probability is conserved. Equivalently, the kinetic operator can be written

$$-\frac{\hbar^2}{2m}\nabla\cdot(e^{-\psi}\nabla) = \frac{1}{2m}\,\hat{p}_\psi^2, \qquad \hat{p}_\psi \equiv -i\hbar\, e^{-\psi/2}\,\nabla\, e^{-\psi/2}, \tag{8}$$

which is self-adjoint on the natural domain (e.g. square-integrable functions with appropriate boundary conditions) under the flat measure. For bounded domains, impose Dirichlet or Neumann conditions on Ψ; for $\mathbb{R}^3$ require $\Psi, \nabla\Psi \in L^2$ with $e^{-\psi}$ bounded and positive.

IV. LABORATORY DISCRIMINATOR

While the theoretical resolution is complete, *experimental verification remains the decisive test of which theory nature follows.* In a nondispersive band, an evacuated cavity with frequency $f_{\rm cav} \propto c_1/L$ and a co-located atomic clock $f_{\rm at}$ respond differently to ψ. Across an altitude change Δh,

$$\frac{\Delta R}{R} = \xi\frac{\Delta\Phi}{c^2}, \qquad R \equiv \frac{f_{\rm cav}}{f_{\rm at}}. \tag{9}$$

In GR, $\xi = 0$; in DFD, $\xi \simeq 1$ [18]. For Earth's surface,

$$\frac{\Delta R}{R} \approx 1.1\times10^{-14} \text{ per 100 m}. \tag{10}$$

This level is achievable with state-of-the-art optical metrology [7, 8]. Matter-wave interferometry provides a second discriminator: DFD predicts a T^3 phase scaling in long-baseline atom interferometers, yielding a $\sim 2\times10^{-11}$ rad signal at $T = 1$ s, within reach of current facilities [17].

A. GLS $4\to3$ slope extraction (sector-resolved)

Using two cavity materials (e.g. ULE, Si) and two atomic species (e.g. Sr, Yb), form four ratios $R^{(M,S)} = f_{\rm cav}^{(M)}/f_{\rm at}^{(S)}$ at two altitudes. The observable slopes are $\Delta R/R = \xi^{(M,S)}\,\Delta\Phi/c^2$ with $\xi^{(M,S)} = \alpha_w - \alpha_L^{(M)} - \alpha_{\rm at}^{(S)}$. A generalized least squares (GLS) fit over the four slopes identifies the three combinations $(\delta_{\rm tot}, \delta_L, \delta_{\rm at})$ with internal consistency and covariance control:

$$\delta_{\rm tot} \equiv \alpha_w - \alpha_L^{\rm ULE} - \alpha_{\rm at}^{\rm Sr}, \quad \delta_L \equiv \alpha_L^{\rm Si} - \alpha_L^{\rm ULE}, \quad \delta_{\rm at} \equiv \alpha_{\rm at}^{\rm Yb} - \alpha_{\rm at}^{\rm Sr}. \tag{11}$$

GR predicts all three δ's vanish; DFD predicts a nonzero $\delta_{\rm tot}$ in a nondispersive band.

V. DISCUSSION

A. Collapse models (GRW/CSL) vs. DFD

GRW and CSL add stochastic, non-unitary collapse terms to resolve the GR/QM tension [6]. DFD requires no such postulates: the background is a classical c-number field ψ, so there is never more than one geometry to begin with. Penrose's structural paradox is absent without modifying the Schrödinger equation stochastically.

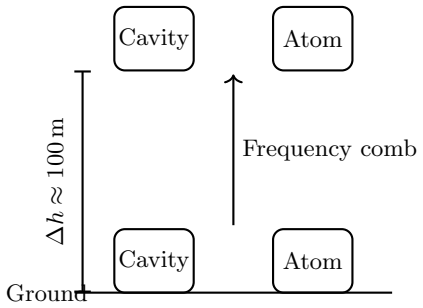

FIG. 3. Sector-resolved cavity–atom LPI test: GR predicts zero slope, DFD predicts $\Delta R/R \sim 10^{-14}$ per 100 m.

TABLE II. How different approaches treat superposed mass distributions.

Approach	Geometry in superposition	Resolution mechanism
GR + QM	Two spacetimes	Structural paradox (Penrose)
GRW/CSL	One spacetime	Stochastic collapse postulate
Decoherence	Two spacetimes	Environment hides interference
DFD	One ψ field	Convex-sum sourcing; unique PDE

B. Decoherence vs. DFD

Environmental decoherence suppresses interference but does not remove the two-geometry issue in GR. DFD never produces branch geometries: superposed sources create one ψ fixed by ρ_{eff}. Thus decoherence is relevant to experimental visibility, not to resolving a structural inconsistency.

C. Cosmological implications

The same optical-metric mechanism impacts cosmography: line-of-sight inhomogeneities bias optical distances, inducing a directional H_0 anisotropy tied to ψ-weighted density gradients [13]. This links laboratory falsification to large-scale observables.

D. Comparison with other approaches

VI. PENROSE PARADOX VS. DFD (SCHEMATIC)

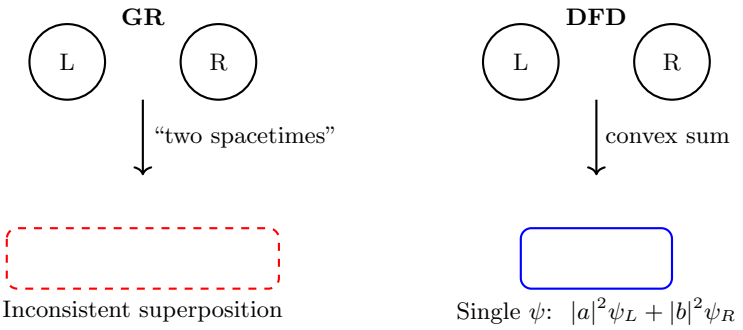

FIG. 4. Schematic contrast. In GR, superposed matter implies two geometries (paradox). In DFD, the scalar ψ is unique, formed from the weighted density distribution.

VII. WELL-POSEDNESS (EXISTENCE & UNIQUENESS)

Theorem (well-posedness). Let $\mu : \mathbb{R}^+ \to \mathbb{R}^+$ be continuous, monotone increasing, and satisfy $0 < \mu_{\min} \le \mu(\cdot) \le \mu_{\max} < \infty$ on compact subdomains of interest. Given $\rho \in L^2_{\rm loc}$ and suitable boundary conditions, Eq. (1) admits a unique weak solution $\psi \in W^{1,2}_{\rm loc}$.

Sketch. Define the energy functional $E[\psi] = \int d^3x\, \mathcal{F}(|\nabla\psi|) - \frac{8\pi G}{c^2}\psi(\rho - \bar\rho)$ with $\mathcal{F}'(y) = \mu(y/a_\star)y$. Monotonicity of μ implies convexity of $\mathcal{F}$ and coercivity on appropriate Sobolev spaces. The direct method of the calculus of variations yields a minimizer; uniqueness follows from strict convexity [9]. For $\mu \to 1$ one recovers the linear Poisson theory; for $\mu \sim x$ deep-field scaling holds.

VIII. CONCLUSION

Penrose's paradox arises only if mass superpositions imply multiple geometries. In DFD, superpositions source one classical ψ field, ensuring consistency with quantum mechanics. The debate moves from philosophy to experiment: a co-located cavity–atom comparison at two altitudes, together with matter-wave interferometry, can decide between GR and DFD with current precision.

Appendix A: Continuity and Hermiticity (derivation details)

Starting from (5), multiply by Ψ^* and subtract the conjugate equation:

$$\Psi^* i\hbar\partial_t\Psi - \Psi(-i\hbar\partial_t\Psi^*) = -\frac{\hbar^2}{2m}\Big[\Psi^*\nabla\cdot(e^{-\psi}\nabla\Psi) - \Psi\nabla\cdot(e^{-\psi}\nabla\Psi^*)\Big]. \tag{A1}$$

Using $\nabla\cdot(f\boldsymbol{A}) = f\,\nabla\cdot\boldsymbol{A} + \nabla f\cdot\boldsymbol{A}$ and rearranging gives $\partial_t|\Psi|^2 + \nabla\cdot\boldsymbol{J} = 0$ with $\boldsymbol{J}$ as in (6). Writing the kinetic operator as $\frac{1}{2m}\hat p_\psi^2$ with $\hat p_\psi = -i\hbar e^{-\psi/2}\nabla e^{-\psi/2}$ shows self-adjointness on the natural domain (Dirichlet/Neumann for bounded regions; L^2 decay at infinity).

Appendix B: Existence/Uniqueness (variational details)

Let $\mathcal{A}(\psi) = \nabla\cdot(\mu(|\nabla\psi|/a_\star)\nabla\psi)$. Assuming μ monotone and bounded away from zero, $\mathcal{A}$ is uniformly elliptic. The functional $E[\psi]$ is convex and coercive, admitting a minimizer; Gateaux differentiability yields (1) in weak form; strict convexity implies uniqueness [9].

[1] R. Penrose, "On gravity's role in quantum state reduction," Gen. Rel. Grav. **28**, 581 (1996).
[2] R. Penrose, *Fashion, Faith, and Fantasy in the New Physics of the Universe* (Princeton University Press, 2014).
[3] C. M. Will, *Theory and Experiment in Gravitational Physics*, 2nd ed. (Cambridge University Press, 2018).
[4] R. M. Wald, *General Relativity* (University of Chicago Press, 1984).
[5] C. Kiefer, *Quantum Gravity* (Oxford University Press, 2007).
[6] A. Bassi, K. Lochan, S. Satin, T. P. Singh, and H. Ulbricht, "Models of wave-function collapse, underlying theories, and experimental tests," Rev. Mod. Phys. **85**, 471 (2013).
[7] A. D. Ludlow, M. M. Boyd, J. Ye, E. Peik, and P. O. Schmidt, "Optical atomic clocks," Rev. Mod. Phys. **87**, 637 (2015).
[8] C. W. Chou, D. B. Hume, T. Rosenband, and D. J. Wineland, "Optical clocks and relativity," Science **329**, 1630 (2010).
[9] L. C. Evans, *Partial Differential Equations*, 2nd ed. (AMS, 2010).
[10] D. Giulini and A. Großardt, "Gravitationally induced inhibitions of dispersion of wave packets," Class. Quantum Grav. **28**, 195026 (2011).
[11] S. Bose, A. Mazumdar, G. W. Morley, *et al.*, "Spin entanglement witness for quantum gravity," Phys. Rev. Lett. **119**, 240401 (2017).
[12] C. Marletto and V. Vedral, "Gravitationally-induced entanglement between two massive particles is sufficient evidence of quantum effects in gravity," Phys. Rev. Lett. **119**, 240402 (2017).
[13] G. Alcock, "Density Field Dynamics: Completing Einstein's 1911–12 Variable-c Program with Energy-Density Sourcing and Laboratory Falsifiability," Zenodo: 17118387 (2025).

[14] G. Alcock, "Sector-Resolved Test of Local Position Invariance with Co-Located Cavity–Atom Frequency Ratios," preprint (under review at *Metrologia*), Zenodo record forthcoming (2025).
[15] G. Alcock, "Strong Fields and Gravitational Waves in Density Field Dynamics: From Optical First Principles to Quantitative Tests," Zenodo: 17115941 (2025).
[16] G. Alcock, "Density Field Dynamics and the c-Field: A Three-Dimensional, Time-Emergent Dynamics for Gravity and Cosmology," Zenodo: 16900767 (2025).
[17] G. Alcock, "Matter-Wave Interferometry Tests of Density Field Dynamics," Zenodo: 17150358 (2025).
[18] G. Alcock, "A Sharp, Testable Slope Prediction for a Sector-Resolved Cavity–Atom LPI Test," preprint (2025).